

Hybrid Piezoelectric-Magnetic Neurons: A Proposal for Energy-Efficient Machine Learning

William Scott¹, Jonathan Jeffrey¹, Blake Heard¹, Dmitri Nikonov², Ian Young², Sasikanth Manipatruni², Azad Naeemi¹, Rouhollah Mousavi Iraei¹

¹Department of Electrical and Computer Engineering, Georgia Institute of Technology, Atlanta, GA, USA, iraei@gatech.edu

²Components Research Group, Intel Corporation, Hillsboro, OR, USA

Abstract

This paper proposes a spintronic neuron structure composed of a heterostructure of magnets and a piezoelectric with a magnetic tunnel junction (MTJ). The operation of the device is simulated using SPICE models. Simulation results illustrate that the energy dissipation of the proposed neuron compared to that of other spintronic neurons exhibits 70% improvement. Compared to CMOS neurons, the proposed neuron occupies a smaller footprint area and operates using less energy. Owing to its versatility and low-energy operation, the proposed neuron is a promising candidate to be adopted in artificial neural network (ANN) systems.

I. Introduction

Deep learning enabled by developments in artificial neural networks (ANNs) has attracted special attention in recent years [32]. Cognitive learning researchers have used ANNs to simulate the natural learning process of the brain and improve the precision of speech recognition, the accuracy of pattern finding, and the reliability of self-driving cars [1, 4, 9, 11, 22]. Modern computer architectures struggle to emulate an ANN, even when processing on highly parallelized GPU architectures [7], [23]. To circumvent this challenge, researchers have turned to investigate how to integrate neural networks directly into hardware. Implementing ANNs as conventional CMOS hardware reduces the power consumption by three orders of magnitude [19]. Even with these improvements, CMOS neuron implementations are inefficient in energy consumption and die area, leading to increasing interest in beyond-CMOS devices for implementing neurons. Most notably, spin-based devices have been proposed as artificial neurons with simpler structure and lower energy consumption than their CMOS counterparts [17], [24]. These spintronic devices have shown to holistically mimic properties of neurons, providing advantages in circuit simplicity, adaptability, and energy efficiency [26]. Moreover, spintronic devices inherently offer non-volatile memory [5], [31]. ANNs need stored information for synaptic weights between communicating neurons; thus, having memory coupled with the circuit reduces energy dissipation and memory bandwidth, helping circumvent the von Neumann bottleneck.

Several spin-based neurons are implemented using tunnel magnetoresistance (TMR) in magnetic tunnel junctions (MTJs) [35] coupled with various phenomena such as domain-wall (DW) motion [3], [27], spin transfer torque (STT) generated by lateral spin valves (LSVs) [17], [28], and spin-Hall effect (SHE) [27], [10]. While these devices are proven to mimic neural properties, some

of their inherent drawbacks must be addressed. The slow switching speed of DW-based neurons prohibits them from being an ideal candidate for the fast implementation of a neuron. To provide non-reciprocity for the LSV neuron, the output magnet is preset by 90° reorientation to its saddle point of energy profile using the STT, generated by preset spin currents. However, the large required current yields substantial energy dissipation in the device. Recent studies on the magnetostriction-assisted all-spin logic (MA-ASL) device, a novel spin valve proposal made of a hybrid structure of magnets and piezoelectrics, have shown the reduction of switching energy by two orders of magnitude [12], [13]. The switching energy can be reduced in an MA-ASL device by employing a 90° magnetostrictive switching, experimentally demonstrated in [34] and shown to be more robust to thermal noise [16]. Using these recent advances, this paper proposes a spin-based neuron based on an MA-ASL device and an MTJ. The proposed structure integrates the advantages of previously proposed spintronic neurons with those of MA-ASL creating a structure that can be implemented into large-scale ANNs.

The rest of the paper is organized into three sections. Section II details the operation of the proposed device. Section III shows how the proposed device integrates into larger circuit schemes. Section IV analyzes the performance of the device. Finally, in section V we conclude the paper.

II. Behind the MA-ASL Device

Figure 1 displays the structure of a simple MA-ASL device [13], made of the input magnet, Magnet 1, and the output magnet, Magnet 2, with each resting on top of a piezoelectric layer and connected by a metallic (Cu) interconnect. Both Magnet 1 and 2 have an easy axis along the $\pm x$ direction; meaning the energy profile of magnets is lower at these directions. To reorient the output magnet, a voltage is applied across the thickness of the piezoelectric layer to create an anisotropic strain along the y axis inside the piezoelectric layer transferred to Magnet 2. This strain couples to the magnetization through the magnetoelastic energy of the magnet; hence, the easy axis of the magnet rotates by 90°; thus, Magnet 2 reorients from the $+x$ direction to the $\pm y$ direction.

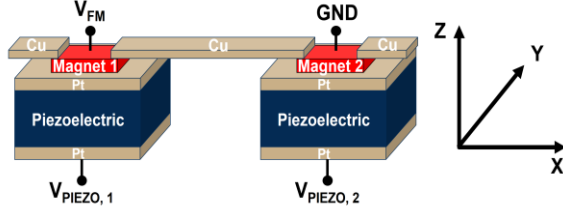


Figure 1. Schematic of the MA-ASL device.

Once $V_{PIEZO,2}$ switches back to low, the easy axis will rotate back to the $\pm x$ direction, which briefly leave Magnet 2 at the meta-stable saddle point, making it equally likely to switch to the $+x$ or $-x$ directions. We break the symmetry by applying a spin-polarized current to Magnet 2 generated by an electrical current passing through Magnet 1; thus, the final magnetization is determined by the orientation of the spin current in either $+x$ or $-x$ directions. For instance, if a spin current with an orientation opposite to Magnet 1 is created by passing a current through the magnet to ground, the spin current will travel down the spin valve. This spin current applies an STT to Magnet 2, then Magnet 2 rotates to the $-x$ direction after $V_{PIEZO,2}$ goes low, making the device act as an inverter.

The physics behind the MA-ASL involves the magnetization dynamics of magnets, governed by the Landau-Lifshitz-Gilbert (LLG) equation,

$$\frac{d\vec{m}}{dt} = -\gamma\mu_0[\vec{m} \times \vec{H}_{eff}] + \alpha \left[\vec{m} \times \frac{d\vec{m}}{dt} \right] + \frac{\vec{I}_{s,\perp}}{qN_s}. \quad (1)$$

The magnetic orientation is represented by \vec{m} , and its change is related to $\vec{I}_{s,\perp}$, the perpendicular spin current, and N_s , the number of spins in the magnet. In (1), μ_0 , α , and γ represent the free space permeability, the Gilbert damping coefficient, and the gyromagnetic ratio, respectively [4], [29]. \vec{H}_{eff} represents the net magnetic field, which is the sum of the uniaxial anisotropy field, \vec{H}_U , the demagnetization field, \vec{H}_{demag} , and the thermal noise field, $\vec{H}_{thermal}$ [5]. Anisotropy and magnetoelastic energy are intertwined; thus, \vec{H}_U is created due to the changes in the magnetoelastic energy, E_{ME} [24],

$$E_{ME} = \frac{-3}{2}\lambda Y \left[\left(m_x^2 - \frac{1}{3} \right) \epsilon_{xx} + \left(m_y^2 - \frac{1}{3} \right) \epsilon_{yy} + \left(m_z^2 - \frac{1}{3} \right) \epsilon_{zz} \right]. \quad (2)$$

The magnetostrictive coefficient and Young's modulus are represented by λ and Y , respectively. The magnetization components are represented with m_x , m_y , and m_z , while the components of strain are represented with ϵ_{xx} , ϵ_{yy} , and ϵ_{zz} along the x , the y , and the z axes, respectively. The net applied strain to the magnet, $\epsilon_{xx} - \epsilon_{yy}$, is derived using

$$\epsilon_{xx} = \epsilon_0 + d_{31} \frac{V_{PIEZO,2}}{t}, \quad (3)$$

$$\epsilon_{yy} = \epsilon_0 + d_{32} \frac{V_{PIEZO,2}}{t}. \quad (4)$$

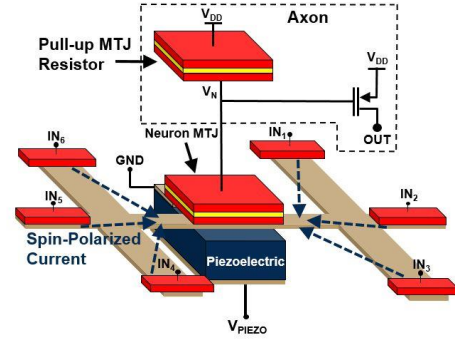


Figure 2. Proposed MA-ASL neuron, shown with six inputs. The net spin current in the interconnect applies STT to the free layer of the neuron MTJ in timing with the piezo clock, switching the orientation of the neuron output.

In these equations, d_{31} and d_{32} are piezoelectric constants [13], $V_{PIEZO,2}$ is the voltage applied across the piezoelectric layer, and t is the piezoelectric thickness.

To simulate the operation of the MA-ASL device, magnets, metallic channels, and piezoelectric layer are modeled as building blocks that are solved self-consistently using SPICE [12], [13]. These models account for the change in the magnetoelastic energy of magnets as an equivalent anisotropy field [12], [13]. The magnetization dynamics and the spin current transport in metallic channels are accounted using the SPICE models developed by Bonhomme et al. in [5]. The magnetization dynamics is calibrated with numerical methods implemented by MATLAB in [5]. The current transport models are calibrated with experimental results [20].

III. Spin Neuron Proposal

A. Neuron Functionality

The proposed neuron, shown in Figure 2, is a modified MA-ASL structure whose output magnet is the free magnetic layer of an MTJ. The input voltages, shown for six inputs (IN_1 – IN_6) in Figure 2 as an example, produce charge currents that flow through the corresponding input magnets and become spin-polarized at the interfaces with the metallic channel. These spin-polarized currents combine below the output magnet according to the sum,

$$I_{s,out} = \sum_j I_{s,j} = \sum_j \eta_j e^{-\frac{L_j}{L_{SRL,j}}} I_{c,j}, \quad (5)$$

where $I_{s,out}$ is the spin current injected into the output magnet, $I_{s,j}$'s are the spin current contributions from each magnet j , and $I_{c,j}$'s are the input charge currents [23]. The distance between each input magnet and the output magnet is represented by L_j . The spin polarization at the interface of each magnet and channel is represented by η_j . The spin relaxation length, $L_{SRL,j}$, is affected by the grain boundary and sidewall scattering due to size effects and material properties of the metallic channel [12].

The net injected spin current, $I_{s,out}$, applies an STT to the output magnet. If strong enough, the STT will rotate the output magnetization, \hat{m}_{out} . The output magnet is in contact with an MgO

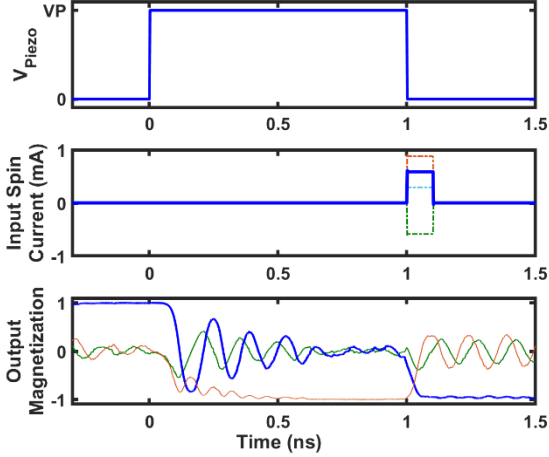


Figure 3. Transient response of the MA-ASL device. In the first phase of operation, V_{PIEZO} turns on for 1 ns as shown in the first graph. The second graph illustrates the second phase of operation, in which STT is applied to the output magnet through the injected net spin current (in blue) from three input magnets (shown with dotted lines), applied after V_{PIEZO} turns off. The third graph shows the magnetization of the output magnet (x , y , and z axes shown in blue, red, and green respectively), and how it is affected by V_{PIEZO} and the spin currents.

layer that separates it from a magnet fixed in the $+x$ direction, forming a three-layer MTJ. As the output magnetization changes, the resistance across the MTJ also changes, following the equation,

$$R_{MTJ} = \frac{1+P}{G_P(1+P\hat{m}_{out,x})}, \quad (6)$$

where R_{MTJ} is the resistance of the MTJ, $\hat{m}_{out,x}$ is the x -component of \hat{m}_{out} , and G_P is the conductance of the MTJ in its low-resistance state, the $+x$ direction [23]. The polarization factor, P , is

$$P = \frac{G_P - G_{AP}}{G_P + G_{AP}} = \frac{TMR}{TMR + 2}, \quad (7)$$

where G_{AP} is the conductance of the MTJ in its high-resistance antiparallel state, the $-x$ direction [23]. As shown in Figure 2, the change in the resistance of the MTJ is sensed by connecting the structure to a pull-up resistor connected to V_{DD} ; then, the voltage above the output neuron follows

$$V_N = \frac{R_{MTJ}}{R_{MTJ} + R_{pull-up}} V_{DD}, \quad (8)$$

where $R_{pull-up}$ is the resistance of the pull-up resistor, implemented with an MTJ with two fixed magnetic layers. The voltage, V_N , is amplified by a PMOS transistor, forming the axon where the neuron's output can be transferred to other neurons.

B. Transient Response of the Neuron

The transient response of the magnetization is shown in Figure 3 for a neuron with three inputs. In the first phase of device operation, V_{PIEZO} is pulsed high for a duration of 1 ns, rotating \hat{m}_{out} to the $+y$ or the $-y$ direction. When V_{PIEZO} turns off, \hat{m}_{out} will be placed at the saddle-point of the energy profile. In the

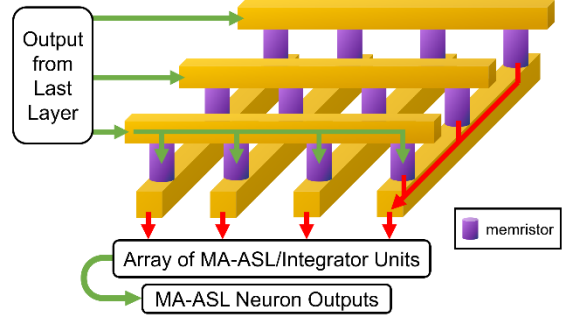


Figure 4. Memristive cross-bar network. The cross-bar array sums together the input currents, abbreviating the number of magnets needed for the output neurons.

Table 1: Performance Comparison of MA-ASL Neuron against its CMOS and Spintronic Counterparts

NEURON DEVICE	Digital CMOS [21]	Analog CMOS [30]	Spintronic [29]	MA-ASL Neuron
DELAY	10 ns	10 ns	1 ns	1.1 ns
ENERGY	832.6 fJ	700 fJ	0.81 fJ	0.25 fJ

second phase of operation, 10x shorter than the first phase, the input voltages are pulsed for 0.1 ns, applying an STT that tips \hat{m}_{out} toward $+x$ or $-x$. The delay of the final switching is inversely proportional to the magnitude of the net spin current, $I_{s,out}$. Compared to an STT-only realignment, this magnetostriction-assisted re-alignment of \hat{m}_{out} onto the axis requires two orders of magnitude lower energy dissipation.

C. Integration into Neural Network

To connect the proposed device into a neural network with machine learning capabilities, we must first show how it mimics a neuron. In Figure 2, the axon of the neuron uses the voltage from the output MTJ as the gate voltage for a PMOS transistor, creating a charge current output. For the synapses, additional circuitry would be required to correctly weight the input current. One proposed method is with a memristive crossbar network, as shown in Figure 4. This structure places memristors between input and output lines to weight the charge current being passed among neurons [15]. In this setup, each output from the previous layer of neurons connects as an input to the crossbar network, which applies synaptic weights and outputs to the next layer of neurons.

IV. Benchmarking Against Competing Technologies

As Figure 3 illustrates, the delay of the MA-ASL neuron is about 1.1 ns, slightly larger than that of the spintronic neuron presented in [27], which claims 1 ns. However, Table 1 demonstrates that the MA-ASL neuron demonstrates 70% improvement in terms of energy over the spintronic neuron [5]; the spintronic neuron uses STT to reorient magnets, while the MA-ASL neuron utilizes a combination of STT and magnetostrictive switching, which results in lower overall energy dissipation. When compared with both analog and digital CMOS neurons, the MA-ASL neuron has

advantages in terms of energy consumption and overall chip area. These advantages are due to a more efficient implementation of a spintronic neuron that requires a lower device count. CMOS neurons require shift registers, sense amplifiers, DRAM, and SRAM, which all require large numbers of transistors [7], whereas spintronic neurons require one MTJ and one magnet for each input, using two orders of magnitude less area than CMOS [29] and three orders of magnitude less energy. These improvements in area and energy consumption enable the proposed device to excel in mimicking a neural network, providing competition to CMOS and other spintronic neural networks in Boolean and non-Boolean computations.

V. Future Work

The efficiency of the proposed neuron in learning tasks can be tested through network-scale simulations. Moreover, beyond characterizing the transient response of a single MA-ASL neuron, a neural network architecture of multiple MA-ASL neurons must be investigated further. A prime candidate for a neural network implementation is a memristive crossbar network due to the inherent learning capabilities of memristors and the lower device

count for the structure, because of elimination of circuitry required for backpropagation [15]. As a result, area and power consumption for a neural network will be reduced. The research on MA-ASL neural network topologies may lead to the implementation of network hierarchies usable for processor design or convolutional networks for deep learning [2], [21].

VI. Conclusion

We proposed a spintronic neuron based on the MA-ASL device and the MTJ. The performance of the neuron is benchmarked against its CMOS and spintronic counterparts in terms of area, delay, and energy dissipation. The MA-ASL neuron operates with less than half the energy compared to its spintronic counterparts by employing magnetostrictive switching along with STT switching. Magnetostrictive switching is expected to further enhance the robustness of the operation of neuron to thermal noise as well. The operation of the device was simulated using SPICE models and the physics behind the operation of the device is well understood.

References

- [1] Amodei, D. et al. 2015. Deep Speech 2: End-to-End Speech Recognition in English and Mandarin. 48, (2015). DOI:https://doi.org/10.1145/1143844.1143891.
- [2] Ankit, A., Sengupta, A., Panda, P. and Roy, K. 2017. RESPARC: A Reconfigurable and Energy-Efficient Architecture with Memristive Crossbars for Deep Spiking Neural Networks.
- [3] Barnes, S.E. 2006. Comment on “theory of current-driven domain wall motion: Spin transfer versus momentum transfer.” *Physical Review Letters*. 96, 18 (2006), 1–4. DOI:https://doi.org/10.1103/PhysRevLett.96.189701.
- [4] Bojarski, M., Del Testa, D., Dworakowski, D., Firner, B., Flepp, B., Goyal, P., Jackel, L.D., Monfort, M., Muller, U., Zhang, J., Zhang, X., Zhao, J. and Zieba, K. 2016. End to End Learning for Self-Driving Cars. (2016), 1–9.
- [5] Bonhomme, P., Manipatruni, S., Iraei, R.M., Rakheja, S., Chang, S.C., Nikonov, D.E., Young, I.A. and Naeemi, A. 2014. Circuit simulation of magnetization dynamics and spin transport. *IEEE Transactions on Electron Devices*. 61, 5 (2014), 1553–1560. DOI:https://doi.org/10.1109/TED.2014.2305987.
- [6] Burr, G.W., Narayanan, P., Shelby, R.M., Sidler, S., Boybat, I., Di Nolfo, C. and Leblebici, Y. 2015. Large-scale neural networks implemented with non-volatile memory as the synaptic weight element: Comparative performance analysis (accuracy, speed, and power). *Technical Digest - International Electron Devices Meeting, IEDM*. 2016–Febru, 408 (2015), 4.4.1–4.4.4. DOI:https://doi.org/10.1109/IEDM.2015.7409625.
- [7] Burr, J.B. 1995. Digital Neural Network Implementations 1 Introduction 2 Classifying VLSI implementations. (1995), 1–48.
- [8] Cui, H., Zhang, H., Ganger, G.R., Gibbons, P.B. and Xing, E.P. 2016. GeePS: scalable deep learning on distributed GPUs with a GPU-specialized parameter server. *EuroSys*. (2016), 1–16. DOI:https://doi.org/10.1145/2901318.2901323.
- [9] Graves, A., Mohamed, A. and Hinton, G. 2013. Speech Recognition with Deep Recurrent Neural Networks. 3 (2013). DOI:https://doi.org/10.1109/ICASSP.2013.6638947.
- [10] Haazen, P.P.J., Murè, E., Franken, J.H., Lavrijsen, R., Swagten, H.J.M. and Koopmans, B. 2013. Domain wall motion governed by the spin Hall effect. *Nature materials*. 12, 4 (2013), 299–303. DOI:https://doi.org/10.1038/nmat3553.
- [11] He, K., Zhang, X., Ren, S. and Sun, J. 2016. Deep Residual Learning for Image Recognition. *2016 IEEE Conference on Computer Vision and Pattern Recognition (CVPR)*. (2016), 770–778. DOI:https://doi.org/10.1109/CVPR.2016.90.
- [12] Iraei, R.M., Bonhomme, P., Kani, N., Manipatruni, S., Nikonov, D.E., Young, I.A. and Naeemi, A. 2014. Impact of dimensional scaling and size effects on beyond CMOS All-Spin Logic interconnects. *2014 IEEE International Interconnect Technology Conference / Advanced Metallization Conference, IITC/AMC 2014*. (2014), 353–356. DOI:https://doi.org/10.1109/IITC.2014.6831833.
- [13] Iraei, R.M., Dutta, S., Manipatruni, S., Nikonov, D.E., Young, I.A., Heron, J.T. and Naeemi, A. 2017. A proposal for a magnetostriction-assisted all-spin logic device. *Device Research Conference - Conference Digest, DRC*. 15, 3 (2017), 2016–2017. DOI:https://doi.org/10.1109/DRC.2017.7999492.
- [14] Iraei, R.M., Kani, N., Dutta, S., Nikonov, D.E., Manipatruni, S., Young, I.A., Heron, J.T. and Naeemi, A. 2017. Clocked Magnetostriction-Assisted Spintronic Device Design and Simulation. (Nov. 2017), 1–6.
- [15] Jo, S.H., Chang, T., Ebong, I., Bhadviya, B.B., Mazumder, P. and Lu, W. 2010. Nanoscale memristor device as synapse in neuromorphic systems. *Nano Letters*. 10, 4 (2010), 1297–1301. DOI:https://doi.org/10.1021/nl904092h.
- [16] Kani, N., Heron, J.T. and Naeemi, A. 2017. Strain-Mediated Magnetization Reversal Through Spin-Transfer Torque. *IEEE Transactions on Magnetics*. 53, 11 (2017). DOI:https://doi.org/10.1109/TMAG.2017.2703898.
- [17] Li, Z. and Zhang, S. 2003. Magnetization dynamics with a spin-transfer torque. *May* (2003), 1–10. DOI:https://doi.org/10.1103/PhysRevB.68.024404.
- [18] Locatelli, N., Vincent, A.F., Mizrahi, A., Friedman, J.S., Vodenicarevic, D., Kim, J.-V., Klein, J.-O., Zhao, W., Grollier, J. and Querlioz, D. 2015. Spintronic Devices as Key Elements for Energy-Efficient Neuroinspired

- Architectures. *Proceedings of the 2015 Design, Automation & Test in Europe Conference & Exhibition*. 1, (2015), 994–999. DOI:<https://doi.org/10.7873/DATE.2015.1117>.
- [19] Pham, P.H., Jelaca, D., Farabet, C., Martini, B., LeCun, Y. and Culurciello, E. 2012. NeuFlow: Dataflow vision processing system-on-a-chip. *Midwest Symposium on Circuits and Systems*. (2012), 1044–1047. DOI:<https://doi.org/10.1109/MWSCAS.2012.6292202>.
- [20] Rakheja, S., Chang, S.C. and Naeemi, A. 2013. Impact of dimensional scaling and size effects on spin transport in copper and aluminum interconnects. *IEEE Transactions on Electron Devices*. 60, 11 (2013), 3913–3919. DOI:<https://doi.org/10.1109/TED.2013.2282615>.
- [21] Ramasubramanian, S.G., Venkatesan, R., Sharad, M., Roy, K. and Raghunathan, A. 2014. SPINDLE: SPINtronic Deep Learning Engine for Large-scale Neuromorphic Computing. *Proceedings of the 2014 International Symposium on Low Power Electronics and Design*. (2014), 15–20. DOI:<https://doi.org/10.1145/2627369.2627625>.
- [22] Ramos, S., Gehrig, S., Pinggera, P., Franke, U. and Rother, C. 2017. Detecting unexpected obstacles for self-driving cars: Fusing deep learning and geometric modeling. *IEEE Intelligent Vehicles Symposium, Proceedings*. (2017), 1025–1032. DOI:<https://doi.org/10.1109/IVS.2017.7995849>.
- [23] Rouhollah Mousavi Iraei, Sasikanth Manipatruni, Dmitri E. Nikonov, Ian A. Young, and A.N. 2017. Electrical-Spin Transduction for CMOS–Spintronic Interface and Long-Range Interconnects. *IEEE Journal on Exploratory Solid-State Computational Devices and Circuits Received*. 3, December (2017), 47–55. DOI:<https://doi.org/10.1109/JXCDC.2017.2706671>.
- [24] Sander, D. 1999. The Correlation Between Mechanical Stress and Magnetic Anisotropy in Ultrathin Films. *Rep. Prog. Phys.* 62, (1999), 809. DOI:<https://doi.org/https://doi.org/10.1088/0034-4885/62/5/204>.
- [25] Schmidhuber, J. 2015. Deep Learning in neural networks: An overview. *Neural Networks*. 61, (2015), 85–117. DOI:<https://doi.org/10.1016/j.neunet.2014.09.003>.
- [26] Sengupta, A. and Roy, K. 2017. Encoding Neural and Synaptic Functionalities in Electron Spin: A Pathway to Efficient Neuromorphic Computing. (2017).
- [27] Sengupta, A., Shim, Y. and Roy, K. 2016. Proposal for an all-spin artificial neural network: Emulating neural and synaptic functionalities through domain wall motion in ferromagnets. *IEEE Transactions on Biomedical Circuits and Systems*. 10, 6 (2016), 1152–1160. DOI:<https://doi.org/10.1109/TBCAS.2016.2525823>.
- [28] Sharad, M., Augustine, C., Panagopoulos, G. and Roy, K. 2012. Proposal For Neuromorphic Hardware Using Spin Devices. (2012).
- [29] Sharad, M., Augustine, C., Panagopoulos, G. and Roy, K. 2012. Spin-based neuron model with domain-wall magnets as synapse. *IEEE Transactions on Nanotechnology*. 11, 4 (2012), 843–853. DOI:<https://doi.org/10.1109/TNANO.2012.2202125>.
- [30] Sharad, M., Fan, D. and Roy, K. 2013. Spin-neurons: A possible path to energy-efficient neuromorphic computers. *Journal of Applied Physics*. 114, 23 (2013), 1–15. DOI:<https://doi.org/10.1063/1.4838096>.
- [31] Sun, J.Z. 2000. Spin-current interaction with a monodomain magnetic body: A model study. *Physical Review B*. 62, 1 (2000), 570–578. DOI:<https://doi.org/10.1103/PhysRevB.62.570>.
- [32] Taylor, G.W. 2017. Deep Multimodal Learning. November (2017). DOI:<https://doi.org/10.1109/MSP.2017.2738401>.
- [33] Wang, K.L., Alzate, J.G. and Khalili Amiri, P. 2013. Low-power non-volatile spintronic memory: STT-RAM and beyond. *Journal of Physics D: Applied Physics*. 46, 8 (2013). DOI:<https://doi.org/10.1088/0022-3727/46/7/074003>.
- [34] Wu, T., Bur, A., Wong, K., Leon Hockel, J., Hsu, C.J., Kim, H.K.D., Wang, K.L. and Carman, G.P. 2011. Electric-poling-induced magnetic anisotropy and electric-field-induced magnetization reorientation in magnetoelectric Ni/(011) [Pb(Mg_{1/3}Nb_{2/3}O₃)(1-x)-[PbTiO₃]_x] heterostructure. *Journal of Applied Physics*. 109, 7 (2011), 2009–2012. DOI:<https://doi.org/10.1063/1.3563040>.
- [35] Yuasa, S., Nagahama, T., Fukushima, A., Suzuki, Y. and Ando, K. 2004. Giant room-temperature magnetoresistance in single-crystal Fe/MgO/Fe magnetic tunnel junctions. *Nature Materials*. 3, 12 (2004), 868–871. DOI:<https://doi.org/10.1038/nmat1257>.